CHEMILUMINESCENCE ANALYSIS OF THE EFFECT OF BUTANOL-DIESEL FUEL BLENDS ON THE SPRAY-COMBUSTION PROCESS IN AN EXPERIMENTAL COMMON RAIL DIESEL ENGINE

by

Simona Silvia MEROLA**, Luca MARCHITTO, Cinzia TORNATORE, and Gerardo VALENTINO
Motors Institute, National Research Council, Naples, Italy

Original scientific paper
DOI: 10.2298/TSCI140329086M

Combustion process was studied from the injection until the late combustion phase in an high swirl optically accessible combustion bowl connected to a single cylinder two-stroke high pressure common rail compression ignition engine. Commercial diesel and blends of diesel and n-butanol (20%: BU20 and 40%: BU40) were used for the experiments.

A pilot plus main injection strategy was investigated fixing the injection pressure and fuel mass injected per stroke. Two main injection timings and different pilot-main dwell times were explored achieving for any strategy a mixing controlled combustion. Advancing the main injection start, an increase in net engine working cycle (>40%) together with a strong smoke number decrease (>80%) and NO_x concentration increase (≅50%) were measured for all pilot injection timings. Compared to diesel fuel, butanol induced a decrease in soot emission and an increase in net engine working area when butanol ratio increased in the blend. A noticeable increase in NO_x was detected at the exhaust for BU40 with a slight effect of the dwell-time.

Spectroscopic investigations confirmed the delayed auto-ignition (~ 60 μs) of the pilot injection for BU40 compared to diesel. The spectral features for the different fuels were comparable at the start of combustion process, but they evolved in different ways. Broadband signal caused by soot emission, was lower for BU40 than diesel. Different balance of the bands at 309 and 282 nm, due to different hydrooxide transitions, were detected between the two fuels. The ratio of these intensities was used to follow flame temperature evolution.

Key words: *combustion, common rail Diesel engine, butanol – diesel fuel blends, optical diagnostics, chemiluminescence*

Introduction

Related to transport field, the increasing importance of shortage fossil oil is inducing more and more attention to the development of higher efficiency engines and to the wide-scale use of renewable fuel. Regarding the Diesel engines, it is consolidated their reliability, durability, and high fuel efficiency. These, advantages are biased by the high emissions of airborne particulate matter (PM). While not considering the Diesel engine as the major contributor to urban

* Corresponding author; e-mail: s.merola@im.cnr.it

carbonaceous aerosols and the reason of bad local air quality as well as global climate change [1, 2], it is evident that Diesel engines emit large volumes of NO_x and smoke (soot), which are hard to be decreased or eliminated simultaneously due to the non-uniform fuel distribution [3]. Noteworthy, reduction in pollutant concentration at the exhaust of compression ignition (CI) engines have been obtained using alternative fuels [4] like biodiesel [5-8], alcohols [9-11], liquefied petroleum gas (LPG) [12, 13] and natural gas [14, 15] used in conventional [16] and dual fuel injection systems [17-19]. Regarding alcohol fuel and biodiesel relationship, it has been demonstrated that the oxygenated structures affect the amount of soot reduction [20-24]. Experimental works concluded that esters (as biodiesel) were less effective in reducing soot precursor levels than alcohols given the same mass fraction of oxygen [25]. Even for these reasons, recently, n-butanol is gaining popularity as a very competitive bio-fuel to be used in Diesel engines. Compared to methanol and ethanol, n-butanol has more advantages as an alternative fuel for internal combustion engines [26-29]; it has a lower auto-ignition temperature than methanol and ethanol, so it can be ignited easier when burned in Diesel engines. Besides, butanol has lower volatility and higher energy density than ethanol and methanol. In addition, butanol is less corrosive and can be blended with diesel fuel without phase separation. Butanol can be produced by fermentation of biomass, such as algae, corn, and other plant materials containing cellulose that could not be used for food and would otherwise go to waste [30-33]. Investigations of n-butanol as fuel within CI engines have been conducted by several research groups to evaluate the effects of butanol blends with conventional diesel fuel on performance, exhaust emissions, and combustion [34-41]. These works demonstrated that diesel-butanol blends (until 40% in volume of n-butanol-BU40) achieved better combustion and brake thermal efficiency, and similar power and torque to diesel fuel. Butanol exhibits values of some of the main fuel properties closer to those of diesel fuel, compared to ethanol and methanol. This explained the better Diesel engine behaviour when higher alcohol blends are used instead of lower alcohol blends. Finally, experiments showed that BU30 can replace diesel fuel in CI engines (without any modification and without significant loss of performance) since long-term Diesel engine tests provided satisfactory results [42]. Regarding exhaust emissions, previous works demonstrated that n-butanol and iso-butanol fuel blended with diesel induced HC emissions increasing, NO_x, CO, and smoke emissions decrease [34, 35, 39, 40]. Similar results were obtained in accelerating conditions for the turbocharged Diesel engines fuelled with 40% n-butanol [43, 44]. In an urban drive cycle HC and CO emissions increased, NO_x emissions decreased with the 40% n-butanol blend. In a highway drive cycle, HC and CO emissions were not significantly impacted, but NO_x emissions showed a slight increase. In addition, an 80% reduction in filter smoke number was observed for the 40% butanol blend. The most important critical point of butanol is the cold start. Previous study reported that the drivability of vehicle decreased noticeably for 40% n-butanol-diesel blend for cold-start urban drive cycle, due to a large reduction of approximately 30% in fuel economy and a significant increase in HC and CO emissions [45-47]. Different results were obtained by the experiments on the diesel-butanol low temperature combustion [38, 48]. These showed that with the increase in n-butanol fraction (until 40%), the ignition delay increased, the NO/NO_2 proportion decreased in an overall slight decrease of NO_x and soot emissions decreased greatly, reaching smoke value close to zero. Finally, at high exhaust gas re-circulation levels, CO and total HC emissions decreased with the increase in butanol fraction.

To resume, butanol cost is still an important disadvantage, but the benefits of the blending with diesel are likewise important. Moreover, butanol can be used in conventional internal combustion engines without the need for components modification including engines equipped with high pressure common rail fuel injection system [34, 41, 49]. The benefits of the

electronic control of butanol-diesel blend injection are mainly linked to the strong reduction of soot exhaust emission. This was obtained by means of the oxygenated structure of the alcohol together with the high injection pressure that accelerates the fuel evaporation, enhances the fuel-air mixing and creates a faster combustion rates [50]. Moreover, as known, by injecting a small amount of fuel as pilot before the main injection, it is possible to reduce the peak heat release rate. Therefore, NO_x emission as well as combustion noise was considerably reduced in comparison to the conventional diesel combustion. The effect of pilot injection on the exhaust emission is related to the injection timing. A long dwell time between pilot and main injection reduces particulate emissions with higher efficiency at high load. On the other hand, at medium-low load, a small dwell time allowed to reduce premixed burn fraction and NO_x.

In spite of the several valid papers on the effects of butanol-diesel blends in CI engines, more data are required to better understand the basic physical and chemical phenomena related to the direct injection and the spray combustion process. The main goal of this work is to improve the basic knowledge of butanol effects on multi-injection spray combustion processes. This experimental information is useful to reach fuel flexibility and NO_x-PM trade off optimization and it represents a fundamental support for kinetic chemical modelling and 1-D to 3-D simulation codes. In details, UV-visible flame emission spectroscopy was applied in the combustion chamber of single cylinder high swirl CI engine equipped with a common rail multi-jets injection system. This optical methodology is a powerful diagnostic because natural emissions of diesel flame consist of both chemiluminescence and soot luminosity [51]. Chemiluminescence is produced by the excitation of the intermediate combustion radicals due to exothermic chemical reactions occurring during the auto-ignition and combustion process [52]. Soot luminosity is caused by the emissions of hot soot particles and it is characterized by a continuous broadband spectrum similar to the Planck black body emission curve [53, 54]. Combustion tests were performed fuelling the optical accessible engine with a commercial diesel (BU00) and with blends of 80% diesel with 20% n-butanol (BU20) and 60% diesel with 40% n-butanol (BU40). Combustion process was studied from the injection until the late combustion phase, fixing the injection pressure at 70 MPa and changing the pilot injection timing. Optical results were correlated with the engine parameters and with exhaust emissions.

Experimental apparatus

The engine used for the experimental activity is an external high swirl optically accessible combustion bowl connected to a single cylinder two-stroke high pressure common rail CI engine. The main engine specifications are listed in tab. 1. The external combustion bowl (50 mm in diameter and 30 mm in depth) is suitable to stabilize, at the end of compression stroke, swirl conditions to reproduce the fluid dynamic environment similar to a real direct injection Diesel engine.

The implication of *cylindrical bowl* is related to the peculiar design of the prototype engine that has a large displacement as an air compressor. The main cylinder, connected to the external *swirled bowl* through a tangential duct, allows to supply compressed air flow to the bowl as the piston approaches top dead center. The air flow, coming from the cylinder, is forced within the combustion chamber by means of the tangential duct. In this way, a counter clockwise swirl flow,

Table 1. Specifications of the engine

Two-stroke single cylinder engine	
Cylindrical bowl (mm × mm)	50 × 30
Bore [mm]	150
Stroke [mm]	170
Connecting rod [mm]	360
Compression ratio	10.1:1
Air supply	Roots blower
Outlet/inlet blower ratio	2.1
Bosch injector nozzle	7/0.141/148°

with the rotation axis about coincident to the symmetry axis of the chamber, is generated. The injector was mounted within this swirled chamber with its axis coincident to the chamber axis. In this way the injected fuel is mixed up through a typical interaction with the swirling air flow. The combustion process starts and mainly goes on in the chamber. After few crank angles the piston moves downward, the flow reverses its motion and the hot gases flow through the tangential duct to the cylinder and finally to the exhaust ports. The combustion chamber provides both a circular optical access (50 mm diameter), on one side of it, used to collect images and a rectangular one (size of 10 × 50 mm) at 90°, outlined on the cylindrical surface of the chamber, used for the laser illumination input. The injection equipment includes a common rail injection system with a solenoid controlled injector located on the opposite side of the circular optical access. The nozzle is a micro-sac 7 hole, 0.141 mm diameter, 148° spray angle nozzle. An external roots blower provided an absolute air pressure at the inlet of 0.21 MPa with a peak pressure within the combustion chamber of 4.9 MPa under motored conditions.

During the spectroscopic investigations, the radiative emissions from the combustion chamber were focused by a 78 mm focal length, f/3.8 UV Nikon objective onto the micrometer controlled entrance slit of a spectrometer (Acton SP2150) with 150 mm focal length and 600 groove/mm grating. The central wavelength of the grating was fixed at 300 nm and 400 nm. From the grating the radiations were detected by an intensified CCD camera (PI-MAX3, Princeton Instruments). The camera had an array size of 1024 × 1024 pixels with a pixel size of 13 × 13 μm and 16-bit dynamic range digitization at 100 kHz. The exposure time was fixed at 42 μs and the dwell time between two consecutive acquisitions was set at 62 μs.

Spectroscopic investigations were carried out in the central region of the combustion chamber, divided in eight locations. Figure 1 shows the sketches of the experimental apparatus for the optical investigations. To enhance signal to noise ratio the 64 spectra of each location were averaged. The flame emission spectra were corrected for the optical set-up efficiency using a deuterium lamp with a highly uniform full spectrum. The wavelength calibration was performed using a mercury lamp. The time evolution of combustion products was evaluated from spectroscopic investigations using a post-processing procedure. For each chemical specie, with well-resolvable narrow emission bands, the height of the band was evaluated after the subtraction of emission background and other species contribution. A software, developed in Labview environment, allowed to simultaneously evaluate the emissions of the selected compounds and

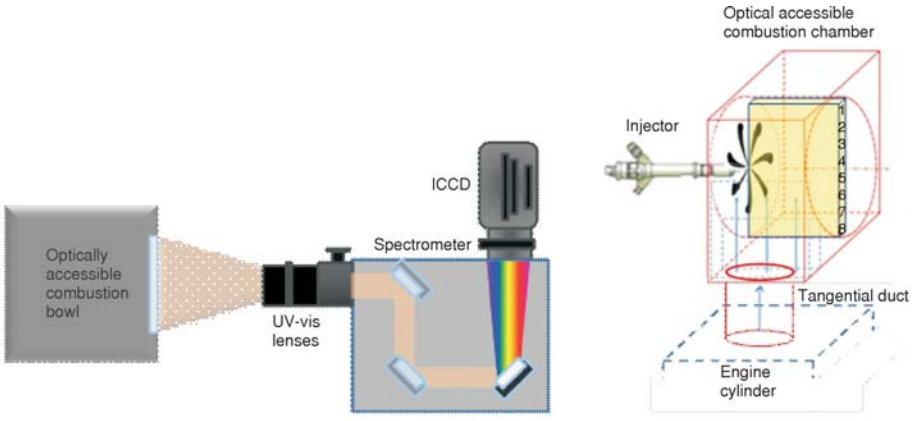

Figure 1. Sketches of the experimental apparatus for the optical investigations. The locations for the spectroscopic investigations are number labelled.

species for each spectrum and time. The hydroxide (OH) and soot emissions were calculated as average on all the spectra. The optical set-up was used also for UV-visible digital imaging of the spray combustion process to support the spectroscopic investigations. In particular, the central wavelength of the spectrometer was fixed at 0 (in this way the device worked as a mirror) and the input slit was opened (3 mm width). The exposure time and the acquisition timing were maintained unchanged.

Table 2. Fuel properties

	BU00	BU20	BU40
Density @15 °C [kgm^{-3}] ASTM D4052	840	830	826
Cetane number ISO4264	52	44	36
Net heat value [MJkg^{-1}]	42.5	41	36.9
Carbon content [%] ASTM D5291	87	80.2	75.19
Hydrogen content [%] ASTM D5291	12.6	15.4	16.8
Oxygen content [%] ASTM D5291	–	4.32	8.64
Initial boiling point [°C] ASTM D86	160	139	117
Distillation 50% vol. [°C] ASTM D86	280	250	226
Distillation 90% vol. [°C] ASTM D86	338	328	325

Combustion tests were carried out using three blends. The baseline fuel was the European low sulphur (10 ppm) commercial diesel with a cetane number of 52 (BU00). Moreover, blends of butanol (20%) – diesel (80%) (by vol.) (BU20) and butanol (40%) – diesel (60%) (BU40) were tested. The main properties of the fuels are reported in tab. 2. All the experimental data were collected using the AVL INDICOM driven by an optical encoder with 0.1 crank angle degree (CAD) resolution. The pressure in the swirl chamber was measured by a quartz pressure transducer AVL QC34C. Results of the in-cylinder pressure were computed over 300 consecutive engine cycles. The NO_x emissions were acquired by an electrochemical sensor, a smoke meter was used for filter smoke number (FSN) measurements. The accuracy of the acquired quantities was 10 ppm for NO_x and 0.1% for smoke.

Results and discussion

Engine parameters and exhaust measurements

Engine tests were carried out at 500 rpm, 30 mg ±1% of fuel was injected at the pressure of 70 MPa setting a single injection (main) and double injections (pilot and main). In the present paper, the start of injection (SOI) indicates the start of the energizing current to the solenoid injector. Because of the hydraulic and electronic delay a shift between the timing of the energizing current to the solenoid SOI and the fuel delivery from the injector nozzles is produced. This delay was estimated in 340 μs from the measurement of the instantaneous fuel flow rate.

Preliminary investigations were performed to evaluate the effect of the fuel injection strategy for reference diesel fuel (BU00) on performance and exhaust emissions. The main SOI was set at 11 and 3 CAD bTDC while the pilot SOI was swept to obtain a pilot-main dwell time of 8, 6 and 4 CAD for both main injections. Figures 2 and 3 show the exhaust measurements (smoke and NO_x). In fig. 4 the engine combustion work *vs.* pilot-main injection dwell crank angle is plotted. The engine combustion work was evaluated as percentage variation of the area under the pressure signal in fired and motored condition [3]. This parameter is correlated to the combustion efficiency of the selected fuel injection strategy.

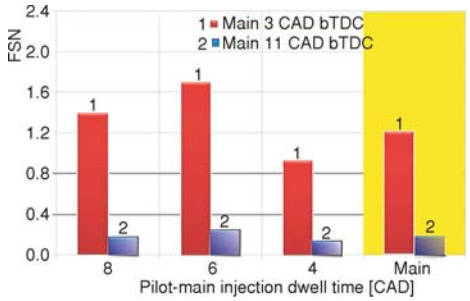

Figure 2. Engine exhaust emissions of smoke, FSN *vs.* pilot-main dwell time for BU00

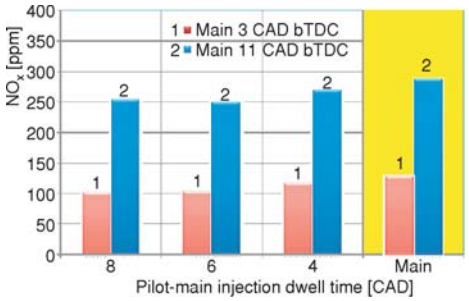

Figure 3. Engine exhaust emissions of NO_x *vs.* pilot-main dwell time for BU00

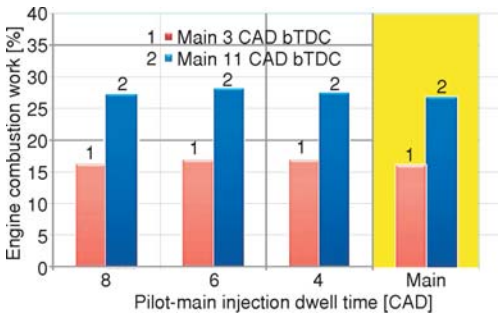

Figure 4. Percentage engine combustion work *vs.* pilot-main dwell time for BU00

Experiments demonstrated that advancing the start of main SOI induced a strong decrease (>80%) in the exhaust smoke for all pilot injection timings. On the other hand, the expected increase in NO_x emission was about 50% and it was matched by an increase in net engine working cycle higher than 40%. All the injection strategies attained the autoignition of the fuel before the end of its delivery from the nozzle, inducing a mixing controlled combustion (MCC) regime. To substantiate this statement, a selection of spray combustion images, detected during the single and double injection strategy fixing the SOI of pilot injection at 17 CAD bTDC, is reported in fig. 5. The investigation was focused on the effect of butanol-diesel blends fixing the main injection at 11 CAD bTDC.

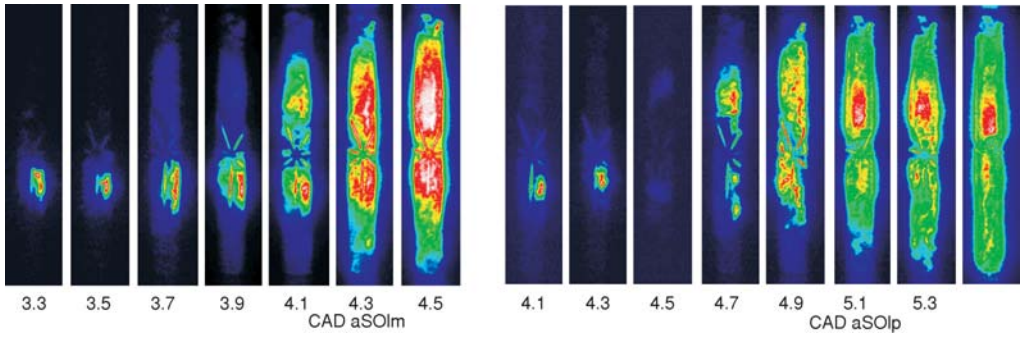

Figure 5. Images detected during the BU00 spray combustion for the single (a) and double (b) injection strategy, setting the pilot injection 17 CAD bTDC. For both cases the main injection occurred at 11 CAD bTDC

Following the previous studying approach, figs. 6, 7, and 8 show smoke and NO_x exhaust emission, and the engine combustion work for diesel and butanol blends fixing the main injection at 11 CAD bTDC at different pilot-main dwell time. Even if the diesel smoke number

resulted already low for diesel, butanol induced a further decrease in soot exhaust emission as butanol blending ratio increased. The effect was expected due to the lower carbon content, the better mixing related to the higher volatility of butanol blends and the presence of oxygen within the butanol molecule. The highest reduction in smoke was obtained setting the dwell time at 6 CAD. The increase in butanol volume fraction produced an appreciable rise in NO_x emissions only for BU40 with a slight effect given by the dwell-time. Regarding the combustion efficiency, the engine combustion work

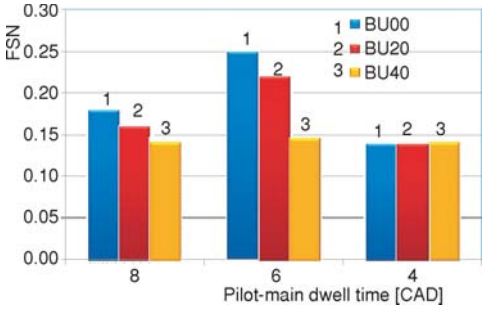

Figure 6. Engine exhaust emissions of smoke, (FSN) *vs.* pilot-main dwell time for selected fuels at fixed SOI of main injection (11 CAD bTDC)

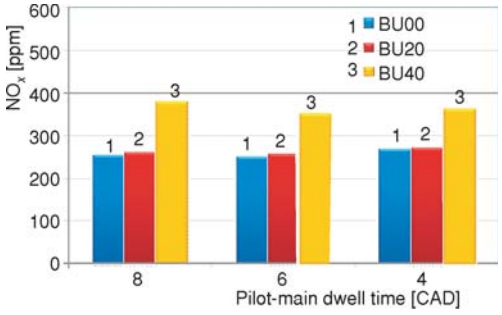

Figure 7. Engine exhaust emissions of NO_x *vs.* pilot-main dwell time for selected fuels at fixed SOI of main injection (11 CAD bTDC)

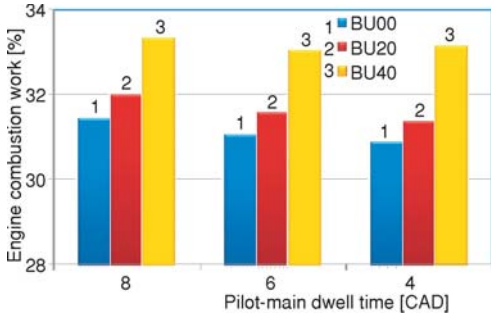

Figure 8. Percentage engine combustion work *vs.* pilot-main dwell time for selected fuels at fixed SOI of main injection (11 CAD bTDC)

increased at higher butanol volume fraction. Again, the increase was influenced by the fuel properties while a minor effect was due to the pilot injection timing. In fact, at higher butanol volume fraction the presence of oxygen within the butanol molecule improve the propensity to form leaner local mixture with a positive impact on soot formation and combustion efficiency.

Optical results

To better understand the fuel injection strategy outcome on the combustion process, natural emission spectroscopy measurements were performed. For brevity, in this work the spectra detected setting the pilot injection at SOI = 17 CAD bTDC are reported. Figure 9 shows the first spectroscopic evidence of combustion process due to the pilot auto-ignition for both fuels. It can be noted that BU40 pilot combustion started around 0.2 CAD after diesel pilot combustion. For both fuels, the pilot auto-ignition was characterised by the OH emissions due to the $A2\Sigma+\rightarrow X2\Pi$ transitions [55]. Many vibrational bands are observable in the UV spectrum, each of them is composed of twelve branches. The most characteristic vibrational transition is (0,0) which begins at 306 nm with its head around 309 nm. Moreover, OH is superimposed on a broadband chemiluminescence, well detectable in diesel spectrum of fig. 9. This was determined by the Vaidya's band system of HCO with highest heads from 290 nm to 360 nm. The Emeleus' bands due to excited formaldehyde molecule CH_2O^* in the range 350-460 nm appeared only as tail of the spectrum [56]. The identification of the Vaidya HC flame band emitters and their formation mechanisms are complex and have been the subject of much reference speculations [57, 58]. Among

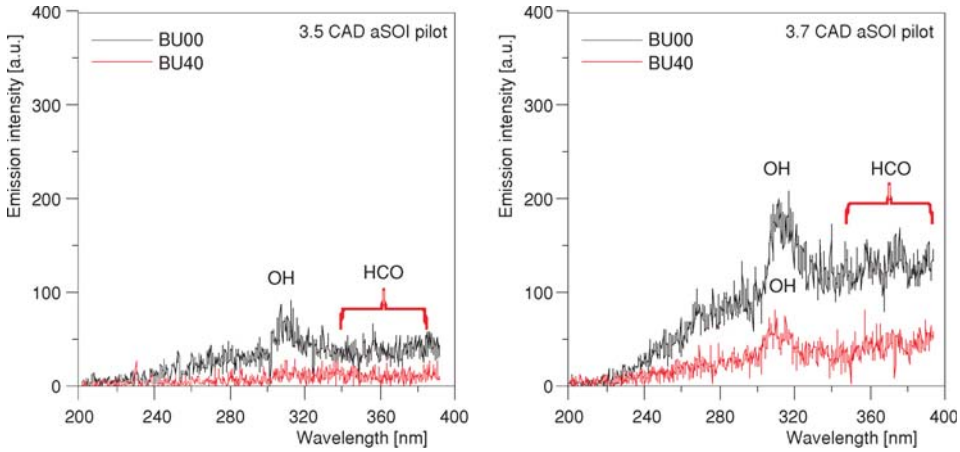

Figure 9. Flame emission spectra detected at the auto-ignition and in the early stage of pilot ignition for BU00 and BU40 (SOI pilot 17 CAD bTDC; SOI main 11 CAD bTDC)

this, it should be noted the reaction of formaldehyde with a free atom or radicals (O, H, OH, or alkyl radical) that induced HCO^* formation [57]. The simultaneous presence of OH and HCO is typical of cool flames. The OH increases in spite of HCO at increasing fuel air ratio value. For rich mixture, CH merged together high HCO and weak OH [57].

After the auto-ignition timing the spectra evolved with similar features. As shown in fig. 10(a), for both fuels at 3.9 CAD aSOI pilot, a weak blue continuum is added to OH and HCO emissions. This emission is due to the chemiluminescence accompanying the re-combination of CO and O [58]:

$$CO(X1\Sigma +) + O(3P) \rightarrow CO_2\ (X1\Sigma + g) + h\nu$$

The CO_2^* emission occurred between 250 and 800 nm with a maximum intensity around 400 nm. As shown in fig. 10(b), in around 0.4 CAD the emission intensity doubled. In particular, the increase in the burned mass fraction and local temperature determined an increase in OH emissions and consequently in the radical concentration.

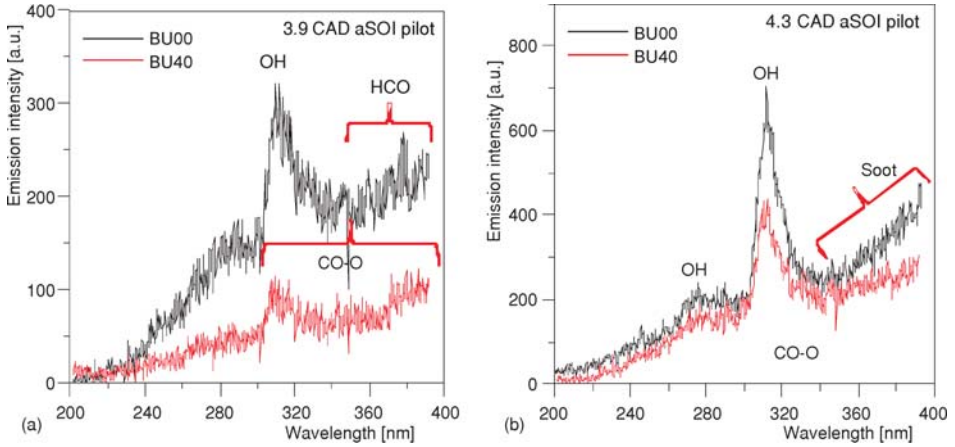

Figure 10. Flame emission spectra detected 4.1 CAD (a) and 4.3 CAD (b) after pilot injection for BU00 and BU40 (SOI pilot 17 CAD bTDC and SOI main 11 CAD bTDC)

Moreover, the 309 nm band due to (0,0) A-X transitions is coupled with the band centred at 282 nm due to (1,0) systems. The two emission bands are more evident for BU00, while for BU40 only the diagonal transition induced a well resolvable emission. Finally, it should be noted that CO_2^* evidence practically remained constant, due to the fast transition to the ground state that induced the increase in neutral molecules [58]. For diesel, at 4.3 CAD aSOI pilot, the spectral evidence of a blue flame emission due to carbonaceous structures and soot nano-precursors was observed [59, 60].

In the early stages of main injection ignition (fig. 11a), the spectral behaviours are quite similar to those observed for pilot-injection ignition for both fuels. The only evident difference is the negligibility of CO_2^* emission contribution and the evidence of a weak signal due to soot produced by the pilot injection combustion.

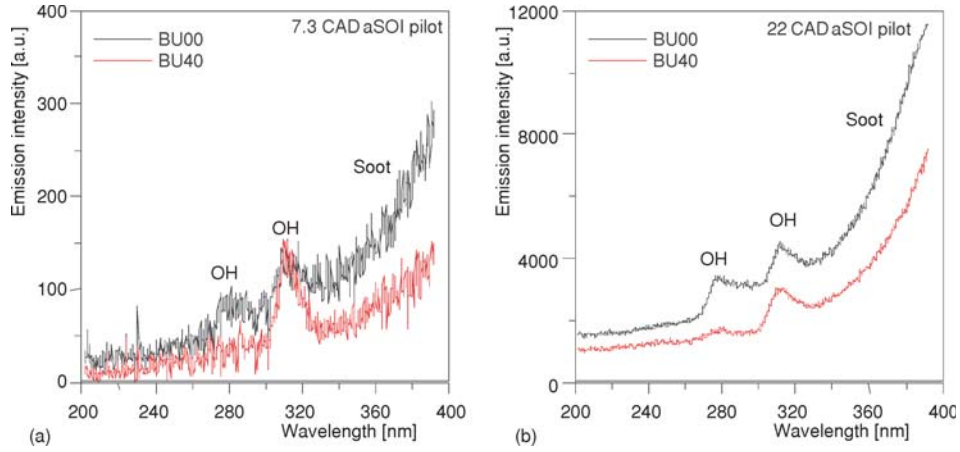

Figure 11. Flame emission spectra detected 7.3 CAD (a) and 22 CAD (b) after pilot injection for BU00 and BU40 (SOIpilot 17 CAD bTDC; SOImain 11 CAD bTDC)

During the main injection combustion, spectra were characterised by a strong soot emission featured by a broadband signal that increased with the wavelength like a blackbody curve, as shown in fig. 11(b) [50, 60]. Soot emission and thus soot concentration was lower for BU40 than diesel. The relative intensity between the two fuels remained unchanged during the combustion process. Moreover, the two OH band systems due to (0,0) and (1,0) A-X system showed comparable emission intensity. This optical evidence persisted until the late combustion phase in which the oxidation mechanism reduced the soot and highlighted the OH emission. The effect is well observable in fig. 12, that shows the spectra detected at 11 CAD aTDC (28 aSOI pilot) for both fuels.

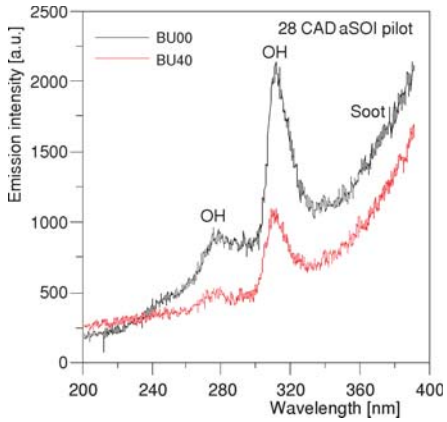

Figure 12. Flame emission spectra detected 28 CAD after pilot injection for BU00 and BU40 (SOI pilot 17 CAD bTDC and SOI main 11 CAD bTDC)

In order to better understand the effect of fuel and injection strategy on the combustion process, the evolutions of soot and OH were calculated. In particular, OH (0,0) emission was measured as height of the 309 nm band system after the subtraction of the emission background, evaluated as the mean value between the emissions measured at 300 nm and 320 nm. Soot emission was evaluated as mean intensity at 500 nm using data obtained with 400 nm central wavelength. The OH and soot evolutions for all the selected conditions are plotted in figs. 13 and 14.

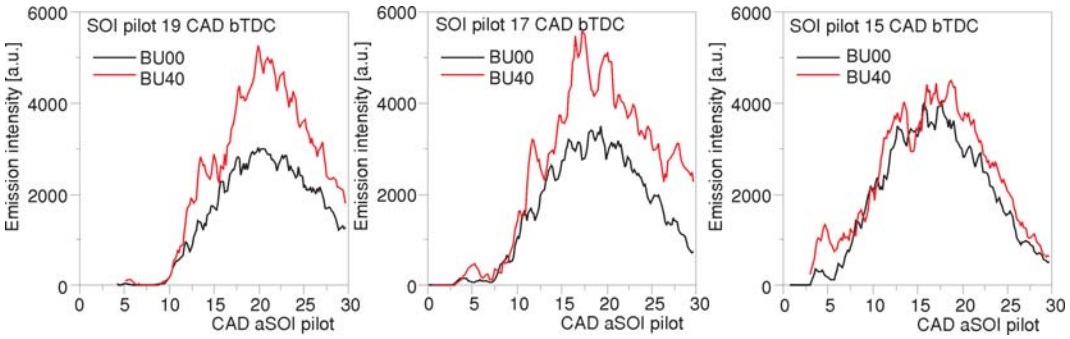

Figure 13. Time evolution of the OH emission (309 nm) for both fuels and the different pilot injection timings

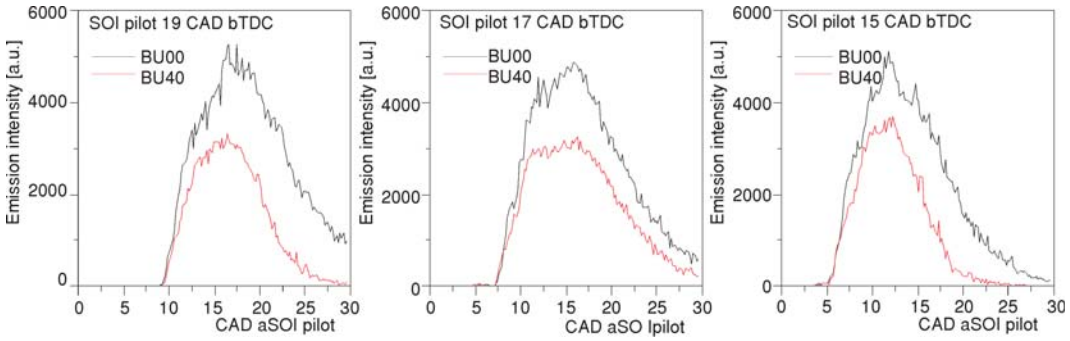

Figure 14. Time evolution of the soot emission for both fuels and the different pilot injection timings

In the OH radical evolution, three phases can be recognized. The first one was due to the pilot ignition, the second one was related to the mixed controlled combustion of the main injection, and the third one occurred after the end of main injection and it was characterized by soot oxidation. The reduction of pilot-main dwell time increased the OH concentration in the early stage of auto-ignition, for both fuels, and the relative signal intensity. This effect was related to the higher pressure and temperature condition in the combustion chamber at delayed pilot injection timing that influenced its auto-ignition. The pilot combustion obviously influenced the main injection combustion. In particular, reducing the dwell time between pilot and main, the combustion main SOI advanced and the OH formation rate increased. As a consequence, the soot formation was reduced by a simultaneous OH oxidation action. Finally, the OH evolution during the main injection combustion gave an inverse behaviour compared to that observed for

the pilot injection combustion. This was due to the higher temperature gradient in the combustion chamber during the main injection combustion. These effects were more highlighted for BU40 due to the oxygen within the butanol molecule. As consequence of these phenomena, soot concentration was lower for BU40, as also confirmed by the exhaust measurements, and the discrepancy between the two fuels decreased with the pilot-main dwell time reduction.

The effect of butanol is well observable in the oxidation phase. This occurred because soot formation, caused by high temperature decomposition, mainly takes place in the fuel-rich zone at high temperature and pressure, specifically within the core region of each fuel spray. If the fuel is partially oxygenated, as it is the case of butanol blends, it has the ability to reduce locally fuel-rich regions and to limit soot formation. Moreover, butanol blends are characterized by lower stoichiometric air-fuel ratio (less air is needed to achieve stoichiometry and consequently complete combustion), which reduces the possibility of existence of fuel-rich regions in the non-uniform air-fuel mixture. Finally, the absence of aromatic compounds in butanol blends reduces the concentration of soot precursors.

Regarding the (1,0) A-X OH emission measured at 282 nm, it can be used together with (0,0) at 309 nm to evaluate the flame temperature. In fact, the line intensities S(T) (cm^{-1}/atm·cm) at the equilibrium temperature T [K] can be expressed:

$$S(T) = \frac{1}{8\pi c\nu^2}\left(\frac{N}{p}\right)\frac{\mathrm{e}^{-\frac{c''E''}{T}}}{Q_{vR}} A_{v''J''}^{v'J'}(2J'+1)(1-\mathrm{e}^{-\frac{c''\nu}{T}}) \tag{1}$$

where $\nu(= E' - E'')$ [cm^{-1}] is the transition frequency, $c = 2.99792458\cdot10^{10}$ cm/s – the light speed, N – the total number of OH molecule per cm^3, p [atm] is the pressure, c'' =1.4388 mK – the second radiation constant; $A_{v''J''}^{v'J'}$ [s^{-1}] – the Einstein coefficient, E'' – the lower state energy, and Q_{vR} – the vibration-rotation partition function [61]. The Q_{vR} is supposed equal to Q_{v} Q_{R}, where the vibrational partition function Q_{v} in the harmonic oscillator approximation is:

$$Q_v = \frac{1}{1-\mathrm{e}^{-\frac{c''\omega_e}{T}}} \tag{2}$$

where ω_{e} is the vibrational harmonic oscillator frequency and it was evaluated ω_{e} = 3737.761 cm^{-1} [62].

In this work, the Einstein coefficients tabulated by Chidsey and Crosley [63] and revised by Goldman and Gillis [64] have been used.

Starting from eq. (1), the ratio between the experimental emission intensities measured at 309 nm and 282 nm allowed to evaluate the quasi-adiabatic flame temperature [65]. The retrieving of combustion temperature from OH chemiluminescence has the great advantage that is free from calibration. On the other hand some drawbacks should be considered: the source of radiation is not in equilibrium, self-absorption and collision quenching can influence the evaluation, and the subtraction of the continuous background due to soot or CO_2^* is necessary.

In this work, combustion temperature obtained for the selected operative conditions are shown in fig. 15. The low intensity of OH emission during the pilot injection ignition, that decreased at increasing pilot-main dwell time, induced a very high uncertainty in the temperature evaluation. This is better estimable during the main injection combustion, in particular during the late phase when the soot is oxidised and OH bands are easier to resolve. Results of fig. 15 demonstrated that flame temperature was lower for BU40 in each fuel injection condition, during the whole combustion process. This was due to the lower C:H atom ratio of alcohols than diesel oil. Even if this contributed to reduce the NO formation rate, the significantly higher oxy-

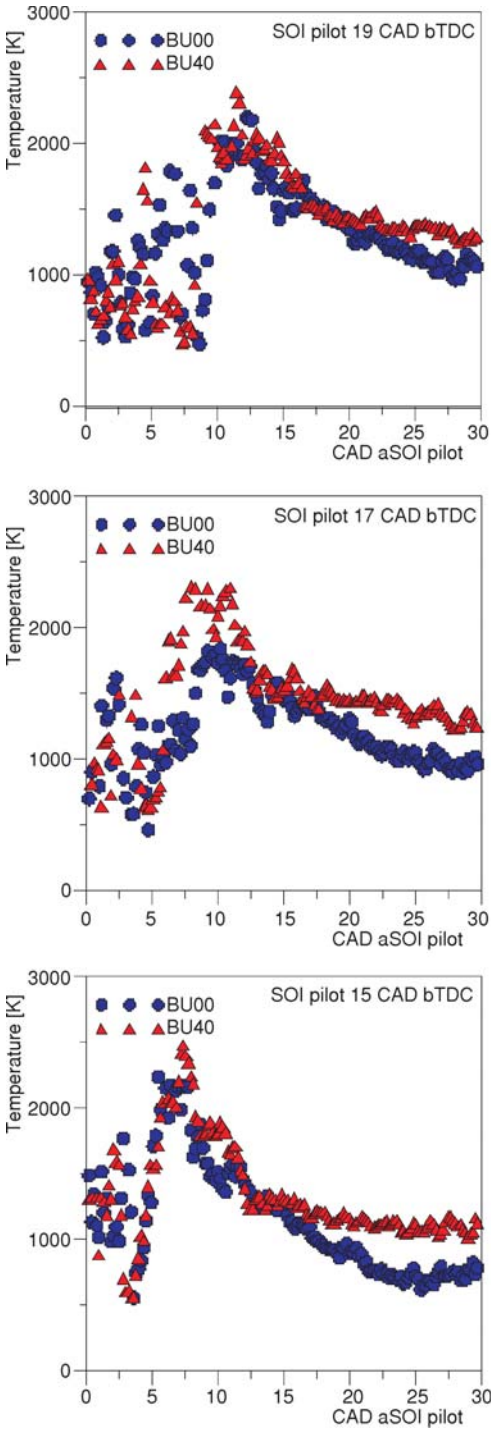

Figure 15. Combustion gas temperature evaluated by A-X OH chemiluminescence

gen availability induced local conditions nearer to stoichiometric compared to the neat diesel fuel operation. This works towards higher NO_x liability, in agreement with the exhaust data.

Conclusions

Fuel spray combustion was investigated in high swirl optically accessible combustion bowl connected to a single cylinder two-stroke high pressure common rail CI engine.

The engine was fuelled with commercial diesel (BU00) and with blends of 80% diesel with 20% n-butanol (BU20) and 60% diesel with 40% n-butanol (BU40).

Combustion process was studied from the injection until the late combustion phase, fixing the injection pressure and fuel mass injected per stroke. The pilot SOI was changed considering two main injection timings. All the tested injection strategies induced a MCC regime.

Experiments demonstrated that advancing the main SOI an increase in engine combustion work (>40%) was achieved. Regarding exhaust emissions, a strong smoke number decrease (>80%) and NO_x concentration increase (≅50%) were measured for all pilot injection timings. Compared to diesel, butanol induced a decrease in soot exhaust emission and an improvement in engine combustion work as butanol blending ratio increased due to the enhanced fuel air mixing and the presence of oxygen within the butanol molecule. These properties improve the propensity to form leaner local mixture with a positive impact on combustion efficiency. An appreciable increase in NO_x emissions was detected for BU40 with a slight effect given by the dwell-time.

Spectroscopic investigations confirmed the delayed auto-ignition (~60 μs) of the pilot injection with BU40 compared to diesel. Even if the spectral features for both fuels resulted comparable at the start of combustion process, they evolved with different behaviours. As expected, broadband signal like a blackbody curve due to soot emission, was lower for BU40 than diesel. Moreover, different balance between the two fuels of the emission bands at 309 nm and 282 nm

due to (0,0) and (1,0) systems of OH A-X transitions were detected in the whole combustion process. The emission intensity ratio due the two band systems was used to follow the flame temperature evolution.

Acknowledgments

The authors thank Alfredo Mazzei from Motors Institute, CNR of Napoli for the layout and set-up of the experiments.

Acronyms

aTDC – after top dead center
bTDC – before top dead center
BU00 – pure commercial fuel
BU20 – commercial fuel blended with 20% of butanol, [vol]
BU40 – commercial fuel blended with 40% of butanol, [vol]
CAD – crank angle degree
CCD – charge-coupled device
FSOI – fuel delivery start of injection
MCC – mixing controlled combustion
PM – particulate matter
SOI – start of injection
aSOI – after start of injection
UV – ultraviolet

References

[1] Ning, Z., *et al*., Black Carbon Mass Size Distributions of Diesel Exhaust and Urban Aerosols Measured using Differential Mobility Analyzer in Tandem with Aethalometer, *Atmospheric Environment, 80* (2013), Dec., pp. 31-40
[2] Sydbom, A., *et al*., Health Effects of Diesel Exhaust Emissions, *Eur Respir J, 17* (2001), 4, pp. 733-746
[3] Heywood, J. B., *Internal Combustion Engines Fundamentals*, McGraw-Hill, New York, USA, 1988
[4] Batmaz, I., The Impact of Using Hydrogen as Fuel on Engine Performance and Exhaust Emissions in Diesel Engines, Energy Sources, *Part A: Recovery, Utilization, and Environmental Effects, 35* (2013), 6, pp. 6556-6563
[5] Gumus, M., Kasifoglu, S., Performance and Emission Evaluation of a Compression Ignition Engine using a Biodiesel (Apricot Seed Kernel Oil Methyl Ester) and its Blends with Diesel Fuel, *Biomass and bioenergy, 34* (2010), 1, pp.134-139
[6] Ng, J. H., *et al*., Advances in Biodiesel Fuel for Application in Compression Ignition Engines, *Clean Technologies and Environmental Policy, 12* (2010), 5, pp. 459-493
[7] Amarnath, H. K., Prabhakaran, P., A Study on the Thermal Performance and Emissions of a Variable Compression Ratio Diesel Engine Fuelled with Karanja Biodiesel and the Optimization of Parameters Based on Experimental Data, *International Journal of Green Energy, 9* (2012), 8, pp. 841-863
[8] Raheman, H., Ghadge, S.V., Performance of Diesel Engine with Biodiesel at Varying Compression Ratio and Ignition Timing, *Fuel, 87* (2008), 12, pp. 2659-2666
[9] Agarwal, A. K., Biofuels (Alcohols and Biodiesel) Applications as Fuels for Internal Combustion Engines, *Prog Energy Combust Sci, 33* (2007), 3, pp. 233-271
[10] Yilmaz, N., Comparative Analysis of Biodiesel Ethanol Diesel and Biodiesel Methanol Diesel Blends in a Diesel Engine, *Energy, 40* (2012), 1, pp. 210-213
[11] Campos-Fernandez, J., *et al*., A Comparison of Performance of Higher Alcohols/Diesel Fuel Blends in a Diesel Engine, *Applied Energy, 95* (2012), Jul., pp. 267-275
[12] Saleh, H. E., Effect of Variation in LPG Composition on Emissions and Performance in a Dual Fuel Diesel Engine, *Fuel, 87* (2008), 13, pp. 3031-3039
[13] Lee, S. W., *et al.*, Combustion Characteristics of LPG and Biodiesel Mixed Fuel in Two Blending Ratios under Compression Ignition in a Constant Volume Chamber, *International Journal of Automotive Technology, 13* (2012), 7, pp. 1149-1157
[14] Korakianitis, T., *et al*., Natural-Gas Fueled Spark-Ignition (SI) and Compression-Ignition (CI) Engine Performance and Emissions, *Progress in Energy and Combustion Science, 37* (2011), 1, pp. 189-112
[15] Hesterberg, T. W., *et al*., A Comparison of Emissions from Vehicles Fueled with Diesel or Compressed Natural Gas, *Environmental Science & Technology, 42* (2008), 17, pp. 6437-6445
[16] Qi, D.H., *et al.*, Performance and Combustion Characteristics of Biodiesel-Diesel-Methanol Blend Fuelled Engine, *Appl Energy, 87* (2010), 5, pp. 1679-1686

[17] Carlucci, A. P., *et al*., Experimental Investigation and Combustion Analysis of a Direct Injection Dual-Fuel Diesel-Natural Gas Engine, *Energy, 33* (2008), 2, pp. 256-263
[18] Selim, M. Y., *et al.*, Improving the Performance of Dual Fuel Engines Running on Natural Gas/LPG by using Pilot Fuel Derived from Jojoba Seeds, *Renewable Energy, 33* (2008), 6, pp. 1173-1185
[19] Papagiannakis, R.G., *et al*., Emission Characteristics of High Speed, Dual Fuel, Compression Ignition Engine Operating in a wide Range of Natural Gas/Diesel Fuel Proportions, *Fuel, 89* (2010), 7, pp.1397-1406
[20] Kohse-Hoeinghaus, K., *et al*., Biofuel Combustion Chemistry: from Ethanol to Biodiesel, *Angew Chem Int Ed., 49* (2010), 21, pp. 3572-97
[21] Song, J. H., *et al*., Comparison of the Impact of Intake Oxygen Enrichment and Fuel Oxygenation on Diesel Combustion and Emissions, *Energy Fuels, 18* (2004), 5, pp. 1282-1290
[22] Lapuerta, M., *et al*., Effect of Biodiesel Fuels on Diesel Engine Emissions, *Progress in Energy and Combustion Science, 34* (2008), 2, pp. 198-223
[23] Venkata Subbaiah, G., Raja Gopal, K., An Experimental Investigation on the Performance and Emission Characteristics of a Diesel Engine Fuelled with Rice Bran Biodiesel and Ethanol Blends, *International Journal of Green Energy, 8* (2011), 2, pp. 2197-2208
[24] Anbarasu, A., *et al*., The Effect of Ethanol Addition in a Biodiesel Operated DI Diesel Engine on Combustion, Performance, and Emission Characteristics, *International Journal of Green Energy, 10* (2013), 1, pp. 90-102
[25] Jung, H., *et al*., Characteristics of SME Biodiesel-Fueled Diesel Particle Emissions and the Kinetics of Oxidation, *Environmental Science & Technology, 40* (2006), 16, pp. 4949-4955
[26] Veloo, P. S., *et al*., A Comparative Experimental and Computational Study of Methanol, Ethanol, and n-Butanol Flames, *Combustion and Flame, 157* (2010), 10, pp. 1989-2004
[27] Chmielewska, A., *et al*., Dielectric Properties of Methanol Mixtures with Ethanol, Isomers of Propanol, and Butanol, *Journal of Chemical & Engineering Data, 54* (2008), 3, pp. 801-806
[28] Mohsen-Nia, M., *et al*., Dielectric Constants of Water, Methanol, Ethanol, Butanol and Acetone: Measurement and Computational Study, *Journal of Solution Chemistry, 39* (2010), 5, pp. 701-708
[29] Safamirzaei, M., *et al*., Modeling the Hydrogen Solubility in Methanol, Ethanol, 1-Propanol and 1-Butanol, *Fluid Phase Equilibria, 289* (2010), 1, pp. 132-39
[30] Qureshi, N., *et al.*, Cellulosic Butanol Production from Agricultural Biomass and Residues: Recent Advances in Technology, In Advanced Biofuels and Bioproducts. Springer, New York, 2013, pp. 247-265
[31] Jang, Y. S., *et al*., Acetone-Butanol-Ethanol Production with High Productivity using Clostridium Acetobutylicum BKM19, *Biotechnology and Bioengineering*, John Wilay and Sons, New York, USA, 2013
[32] Bhandiwad, A., *et al*., Metabolic Engineering of Thermoanaerobacterium Thermosaccharolyticum for Increased n-Butanol Production, *Advances in Microbiology, 3* (2013), 1, pp. 46-51
[33] Xue, C., *et al*., Characterization of Gas Stripping and its Integration with Acetone-Butanol-Ethanol Fermentation for High-Efficient Butanol Production and Recovery, *Biochemical Engineering Journal, 83* (2014), Feb., pp. 55-61
[34] Rakopoulos, D. C., *et al*., Investigation of the Performance and Emissions of Bus Engine Operating on Butanol/Diesel Fuel Blends, *Fuel, 89* (2010), 10, pp. 2781-2790
[35] Rakopoulos D. C., *et al*., Effects of Butanol-Diesel Fuel Blends on the Performance and Emissions of a High-Speed DI Diesel Engine, *Energy Conversion and Management, 51* (2010), 10, pp. 1989-1997
[36] Ozsezen, A. N., *et al.*, Comparison of Performance and Combustion Parameters in a Heavy-Duty Diesel Engine Fueled with Iso-Butanol/Diesel Fuel Blends, *Energy, Exploration & Exploitation, 29* (2011), 5, pp. 525-541
[37] Lujaji, F., *et al*., Experimental Investigation of Fuel Properties, Engine Performance, Combustion and Emissions of Blends Containing Croton Oil, Butanol, and Diesel on a CI Engine, *Fuel, 90* (2011), 2, pp. 505-510
[38] Valentino, G., *et al.*, Experimental Study on Performance and Emissions of a High Speed Diesel Engine Fuelled with n-Butanol Diesel Blends under Premixed Low Temperature Combustion, *Fuel, 92* (2012), 1, pp. 295-307
[39] Chen Z., *et al*., Study on Performance and Emissions of a Passenger-Car Diesel Engine Fueled with Butanol-Diesel Blends, *Energy, 55* (2013), Jun., pp. 638-646
[40] Chen, Z., *et al*., Combustion and Emissions Characteristics of High n-Butanol/Diesel Ratio Blend in a Heavy-Duty Diesel Engine and EGR Impact, *Energy Conversion and Management, 78* (2014), 3, pp. 787-795

[41] Merola, S. S., *et al.*, Combustion Process Investigation in a High Speed Diesel Engine Fuelled with n-Butanol Diesel Blend by Conventional Methods and Optical Diagnostics, *Renewable Energy, 64* (2014), Apr., pp. 225-237
[42] Campos-Fernandez, J., *et al.*, Performance Tests of a Diesel Engine Fueled with Pentanol/Diesel Fuel Blends, *Fuel, 107* (2013), May, pp. 866-872
[43] Rakopoulos, C. D., *et al*., Investigating the Emissions during Acceleration of a Turbocharged Diesel Engine Operating with Bio-Diesel or n-Butanol Diesel Fuel Blends, *Energy, 35* (2010), 12, pp. 5173-5184
[44] Giakoumis, E. G., *et al*., Exhaust Emissions with Ethanol or n-Butanol Diesel Fuel Blends during Transient Operation: A Review, *Renewable and Sustainable Energy Reviews, 17* (2013), Jan., pp. 170-190
[45] Miers, S., *et al*., Drive Cycle Analysis of Butanol/Diesel Blends in a Light-Duty Vehicle, SAE technical paper 2008-01-2381, 2008
[46] Armas, O., *et al*., Pollutant Emissions from Engine Starting with Ethanol and Butanol Diesel Blends, *Fuel Processing Technology, 100* (2012), Aug., pp. 63-72
[47] Rakopoulos, C. D., *et al*., Study of Turbocharged Diesel Engine Operation, Pollutant Emissions and Combustion Noise Radiation During Starting with Bio-Diesel or n-Butanol Diesel Fuel Blends, *Applied Energy, 88* (2011), 11, pp. 3905-3916
[48] Zhang, Q., *et al*., Experimental Study of n-Butanol Addition on Performance and Emissions with Diesel Low Temperature Combustion, *Energy, 47* (2012), 1, pp. 515-521
[49] Yao, M. F., *et al.*, Experimental Study of n-Butanol Additive and Multi-Injection on HD Diesel Engine Performance and Emissions, *Fuel, 89* (2010), 9, pp. 2191-2201
[50] Agarwal, A. K., *et al.*, Effect of Fuel Injection Timing and Pressure on Combustion, Emissions and Performance Characteristics of a Single Cylinder Diesel Engine, *Fuel, 111* (2013), Sep., pp. 374-383
[51] Zhao, H., Ladommatos, N., Engine Combustion Instrumentation and Diagnostics; SAE tehnical paper 2001-01-30, 2001
[52] Dec, J. E., Espey, C., Chemiluminescence Imaging of Autoignition in a DI Diesel Engine, SAE technical paper 982685, 1998
[53] Zhao, H., Ladommatos, N., Optical Diagnostics for Soot and Temperature Measurement in Diesel Engines, *Progress in Energy and Combustion Science, 24* (1998), 3, pp. 221-255
[54] Kosaka, H., *et al*., Two-Dimensional Imaging of Ignition and Soot Formation Processes in a Diesel Flame, *Int. Journal of Engine Research, 6* (2005), 1, pp. 21-42
[55] Dieke, G. H., Crosswhite, H. M., The Ultraviolet Bands of OH, *Fundamental Data. J. Quant. Spectrosc. Radiat. Transfer, 2* (1962), 2, pp. 97-199
[56] Gaydon, A. G., Wolfhard, H. G., Mechanism of Formation of CH, C_2, OH, and HCO Radicals in Flames, *Symposium (International) on Combustion, 4* (1953), 1, pp. 211-218
[57] Fontijn, A., Mechanism of Chemiluminescence of Atomic Oxygen-Hydrocarbon Reactions, Formation of the Vaidya Hydrocarbon Flame Band Emitter, *J. Chem. Phys., 44* (1966), 4, pp. 1702-1707
[58] Gaydon, A. G., *The Spectroscopy of Flames*, John Wiley and Sons, Inc., New York, USA, 1957
[59] Tree, D. R., Svensson, K. I., Soot Processes in Compression Ignition Engines, *Progress in Energy and Combustion Science, 33* (2007), 3, pp. 272-309
[60] Senda, J., *et al.*, Experimental Analysis on Soot Formation Process In DI Diesel Combustion Chamber by use of Optical Diagnostics; SAE technical paper 2002-01-0893, 2002
[61] Hougen, J. T., The Calculation of Rotational Energy Levels and Rotationa/ Line Intensities in Diatomic Molecules, NBS Monograph 115, U.S. Government Printing Office, Washington, D.C. 1970
[62] Huber, K. P., Herzberg, G., *Molecular Spectra and Molecular Structure IV. Constants of Diatomic Molecules*, Van Nostrand Reinhold, New York, USA, 1979
[63] Chidsey, I. L., Crosley, D. R., Calculated Rotational Transition Probabilities for the A-X System of OH, *Journal of Quantitative Spectroscopy and Radiative Transfer, 23* (1980), 2, pp.187-199
[64] Goldman, A., Gillis, J. R., Spectral Line Parameters for the $A2\Sigma \rightarrow X2\Pi(0, 0)$ Band of OH for Atmospheric and High Temperatures, *JQSRT, 25* (1981), 2, pp. 111-135
[65] Kishimoto K., Seki, K., Estimation and Optical Diagnostics of Combustion with High Temperature Air. *Pacific Science Review, 8* (2006), Dec., pp. 49-57

Paper submitted: March 29, 2014
Paper revised: June 26, 2014
Paper accepted: July 11, 2014